Sensitivity of power functions to aggregation: Bias and uncertainty in radar rainfall retrieval

M. G. Sassi[1], H. Leijnse[2], and R. Uijlenhoet[3]

[1]Royal Netherlands Institute for Sea Research, Physical Oceanography, Den Burg, Texel, Netherlands, [2]Royal Netherlands Meteorological Institute, Observations Research, De Bilt, Netherlands, [3]Hydrology and Quantitative Water Management Group, Wageningen University, Environmental Sciences Group, Wageningen, Netherlands

Abstract Rainfall retrieval using weather radar relies on power functions between radar reflectivity Z and rain rate R. The nonlinear nature of these relations complicates the comparison of rainfall estimates employing reflectivities measured at different scales. Transforming Z into R using relations that have been derived for other scales results in a bias and added uncertainty. We investigate the sensitivity of Z-R relations to spatial and temporal aggregation using high-resolution reflectivity fields for five rainfall events. Existing Z-R relations were employed to investigate the behavior of aggregated Z-R relations with scale, the aggregation bias, and the variability of the estimated rain rate. The prefactor and the exponent of aggregated Z-R relations systematically diverge with scale, showing a break that is event-dependent in the temporal domain and nearly constant in space. The systematic error associated with the aggregation bias at a given scale can become of the same order as the corresponding random error associated with intermittent sampling. The bias can be constrained by including information about the variability of Z within a certain scale of aggregation, and is largely captured by simple functions of the coefficient of variation of Z. Several descriptors of spatial and temporal variability of the reflectivity field are presented, to establish the links between variability descriptors and resulting aggregation bias. Prefactors in Z-R relations can be related to multifractal properties of the rainfall field. We find evidence of scaling breaks in the structural analysis of spatial rainfall with aggregation.

1. Introduction

Aggregation or averaging is ubiquitous in multiresolution contexts that often impose wide-ranging scales (in space and time) at the process, model, and observation levels. Averaging nonlinearly related physical quantities generally leads to a discrepancy between the transformation of the mean and the mean of the transformation (i.e., Jensen's inequality). This discrepancy is a bias, a systematic error in the estimator of the mean. Aggregation bias complicates the interpretation of bed-load sediment transport calculations in rivers [*Ferguson*, 2003; *Recking*, 2013], the upscaling of model simulations of nonlinear soil-processes [*Heuvelink and Pebesma*, 2009], the parameterization of soil moisture in coupled land-atmosphere models [*Nykanen and Foufoula-Georgiou*, 2001], and the estimation of hydrological parameters at the catchment scale for varying topographic resolutions [*Moglen and Hartman*, 2001]. Aggregation bias is a key challenge in quantitative estimation of physical observables using indirect techniques that rely on point-scale nonlinear calibrations [e.g., *Berne and Uijlenhoet*, 2007; *Sassi et al.*, 2012a]. Here we investigate the sensitivity of rainfall-retrieval power-functions, known as Z-R relations, to aggregation of high-resolution X-band weather radar data in space and in time.

The retrieval of rainfall employing indirect measurement techniques relies to a large extent on power functions between the instrument's response and the rain rate. At a global scale, precipitation radars on board of satellite missions provide rainfall maps at several kilometer and subdaily resolutions [*Steiner et al.*, 2003]. At the ground, rainfall maps are routinely retrieved with weather radars at higher spatial (∼ one kilometer) and temporal (∼ 5 min) resolutions. The relations between measured reflectivity [*Uijlenhoet*, 2001] on the one hand and the attenuation suffered by the signal along its path [*Uijlenhoet and Berne*, 2008] and rain rate on the other hand are assumed to be nonlinear power functions. The power function between a measure of signal attenuation and the rain rate is at the core of most retrieval methods based on optical extinction [*Uijlenhoet et al.*, 2011] and microwave attenuation [*Berne and Uijlenhoet*, 2007; *Leijnse et al.*, 2007a,

2007b; *Overeem et al.*, 2011], that typically deliver rainfall rates at even higher temporal resolutions. The nonlinear nature of power functions complicates tallying rainfall estimates from indirect measurements obtained at different resolutions [*Steiner and Smith*, 2004], because retrieving rain rates using relations that have been derived for other spatial and/or temporal scales results in aggregation bias. We show aggregation bias can be corrected for when estimates of the subgrid variability of the radar reflectivity field at the scale of aggregation is taken into account. In that respect, Quantitative Precipitation Estimation (QPE) may benefit from the use of high-resolution spatiotemporal data as it offers the basis for any structural analysis of small-scale rainfall variability.

Rainfall variability is complicatedly tied to climatic, hydrological, and atmospheric processes over widely differing spatiotemporal scales. Identifying a general spatiotemporal statistical structure of precipitation fields is central to approaches involving the analysis, modeling, and observation of rainfall processes. Precipitation fields obey certain scaling power-laws for specific scale ranges [*Fabry*, 1996], which may be transitioned by non power-law scaling regimes [*Marani*, 2005]. Rainfall scaling properties link the statistical moments of precipitation fields with the scale of observation. Approaches based on (multi)fractals [*Lovejoy and Schertzer*, 1990; *Tessier et al.*, 1993] have gained considerable attention in both the temporal [e.g., *Veneziano and Lepore*, 2012] and the spatial [e.g., *Verrier et al.*, 2010; *Mascaro et al.*, 2013] scaling analysis of rainfall structure. Because the fundamental equation of the multifractal formalism involves a power function of the statistical moments with aggregation scale [c.f. *Verrier et al.*, 2013], the formalism may be suitable for understanding and determining the scale dependency of aggregated *Z-R* relations.

For the temporal analysis of disdrometer data, *Verrier et al.* [2013] found the prefactor in *Z-R* relations follows power-law scaling with a break at approximately 4 min. In their analysis, the exponent in *Z-R* relations shows a weak scale dependency when data are nonlinearly regressed or when linear regression of bin averaged data is computed. Overall, their analysis reveals scale dependencies of prefactors in *Z-R* relations can be related to the moment scaling function, which represents the exponent in power functions of the statistical moments with aggregation scale [e.g., *Schertzer and Lovejoy*, 1987; *Gupta and Waymire*, 1990]. Analogous approaches in the spatial domain are less common [*Mandapaka et al.*, 2009] and may be equally relevant for QPE using weather radars. Structural analyses of rainfall variability [*Van de Beek et al.*, 2012] showed shape factors, such as the range and the sill of experimental semivariograms, exhibit scaling in time. In this paper, we show the structural analysis of spatial variability by means of generalized isotropic variograms of order *q* [*Lavallée et al.*, 1993; *Rodriguez-Iturbe and Rinaldo*, 1997] reveals scaling breaks consistent with the spatial analysis based on aggregated *Z-R* relations. Here we systematically use high-resolution radar data to underpin scale-dependencies of *Z-R* relations both in space and time, as opposed to previous studies that have dealt mostly with time series from rain gauges and/or disdrometers.

The objective of this paper is to assess the scale dependencies of *Z-R* relations both in space and in time based on an analysis of high-resolution X-band weather radar data, and to explicitly link the bias due to aggregation with subgrid variability. This paper is organized as follows: Section 2 presents the data analysis and processing methods and introduces the derivation of the bias and uncertainty associated with aggregation based on Taylor series expansions; section 3 presents the results of bias and uncertainty of aggregated data; the behavior of aggregated *Z-R* relations is shown in section 4, whereas the relation to different measures of variability is presented in section 5; we offer a discussion of the results in section 6 and a summary and the conclusions in section 7.

2. Materials and Methods

2.1. Data Source

The data set employed in this study consists of 1 year of radar reflectivity fields measured by the X-band weather radar SOLIDAR, located in Delft, The Netherlands. The radar operated in the 1990s with a radial resolution of 120 m, an angular resolution of $1.875°$, and a temporal resolution of 16 s [*Ligthart and Nieuwkerk*, 1990]. Five events were selected for the analysis and are described in Table 1. More details on these events can be found in *Van de Beek et al.* [2010]. Radar images were corrected for ground clutter, using a static clutter map defined as the exceedance of a threshold value for more than 90% of the time during dry periods. Radar pixels identified as clutter were marked as bad values and no data-gap filling was performed.

Table 1. Description of the Five Events Used in This Study

Event	Description	Legend	Symbol	Date	Time Frame	Accum. (mm)	Max. (mm h^{-1})
1	Light precipitation	LP	Circle	15 May 1993	06:00–08:00	0.6	3
2	Stratiform rainfall	SR	Square	27 May 1993	07:00–09:00	8	16
3	Convective cells	CC	Diamond	16 Sep 1993	10:30–16:00	7	5
4	Squall line	SL	Triangle	21 Sep 1993	02:30–03:30	6	155
5	Weak stratiform precipitation	WSR	Right-pointing triangle	14 Oct 1993	05:00–10:00	9	3.5

As the clutter is static, we do not take these points into account in either the spatial or temporal analysis. Reflectivities were not corrected for attenuation because given the radar's maximum range (~15 km) and the rainfall climatology of the Netherlands [*Uijlenhoet and Berne*, 2008], this was deemed a secondary effect.

2.2. Fitting of Parameters and Transforming From Polar to Cartesian Coordinates
Radar reflectivities were transformed into rain rates assuming a power function with predefined prefactor and exponent ($a=171$ and $b=1.73$ in equation (1), respectively [*Leijnse et al.*, 2008]) to hold at the highest resolution of the radar. Rain rates at highest resolution were subsequently aggregated in time intervals corresponding to scales ranging from 32 s to about 1 h, in powers of two (dyads). A nonlinear regression between aggregated rain rates and aggregated radar reflectivities ($\bar{R}$ and $\bar{Z}$, respectively) was performed for each radar pixel (in total, 128 × 128 pixels per radar image). We chose to perform nonlinear regressions because a linear regression between log ($\bar{R}$) and log ($\bar{Z}$) would yield an additional bias due to the minimization of the squared differences of the log-transformed variables [*Miller*, 1984], and because nonlinear regression generally yields more independent prefactors and exponents [*Verrier et al.*, 2013]. The number of degrees of freedom in the regression decreases with aggregation scale. Therefore, we only performed these analyses for aggregation scales of at most one quarter of the total event duration (see Table 1), up to a maximum of 1 h. The procedure yields a set of 128 × 128 prefactors and exponents, per time scale.

An analogous procedure was adopted in the spatial domain. First, the radar pixels measured in polar coordinates were sampled into a Cartesian grid using a nearest neighbor search based on the Euclidean distance. To find the optimal resolution of the Cartesian grid, we aggregated all pixels in polar coordinates that fall within a given square of predefined size and compared them with the resampled data on a Cartesian grid of the same resolution. Then we repeated the procedure for squares of increasing size, from 100 to 200 m. Figure 1 shows several indicators of the degree of correspondence of radar images in Cartesian and in polar coordinates as a function of the sampling resolution, for the five events in this study. Sampling resolution has a different impact on the comparison depending on the event under consideration. For example, event SL shows the largest Mean Bias for varying sampling rate; this already highlights the physical characteristics of this event such as strong variability and intermittency in space. In general, the degree of correspondence is higher for sampling resolutions of 150 and 175 m. However, we chose to sample radar reflectivities into a Cartesian grid of 125 m resolution because the most frequent Euclidean separation between grid nodes in the polar grid is about 135 m. Radar images sampled in the Cartesian grid were aggregated in squares corresponding to scales ranging from 0.25 to 8 km, in powers of two (dyads). The number of degrees of freedom in the regression remains constant at all scales, whereas the number of radar pixels in aggregated images decreases with aggregation scale. To keep the number of pixels constant across scales, the value corresponding to the coarser scale in aggregated images is kept constant down to the finer scale.

2.3. Theoretical Framework
When the attenuation of the radar signal with range is negligible, rain rates can be retrieved from:

$$Z=aR^b,\tag{1}$$

where Z is radar reflectivity in mm^6 m^{-3}, R is rain rate in mm h^{-1}, and a and b are a prefactor and an exponent, respectively, varying in the ranges 10–1000 and 1–2 [*Battan*, 1973; *Smith and Krajewski*, 1993; *Uijlenhoet*, 2001]. Because $R(Z)$ is a nonlinear function, in general $\mathrm{E}[R(Z)] \neq R(\mathrm{E}[Z])$, with the symbol "E" indicating the statistical expectation. In this context, aggregation effectively means taking expectations over an ensemble of radar reflectivity measurements. This analysis is therefore limited to linear aggregation and nonlinear effects associated with e.g., antenna patterns are disregarded. Furthermore, we assume equation
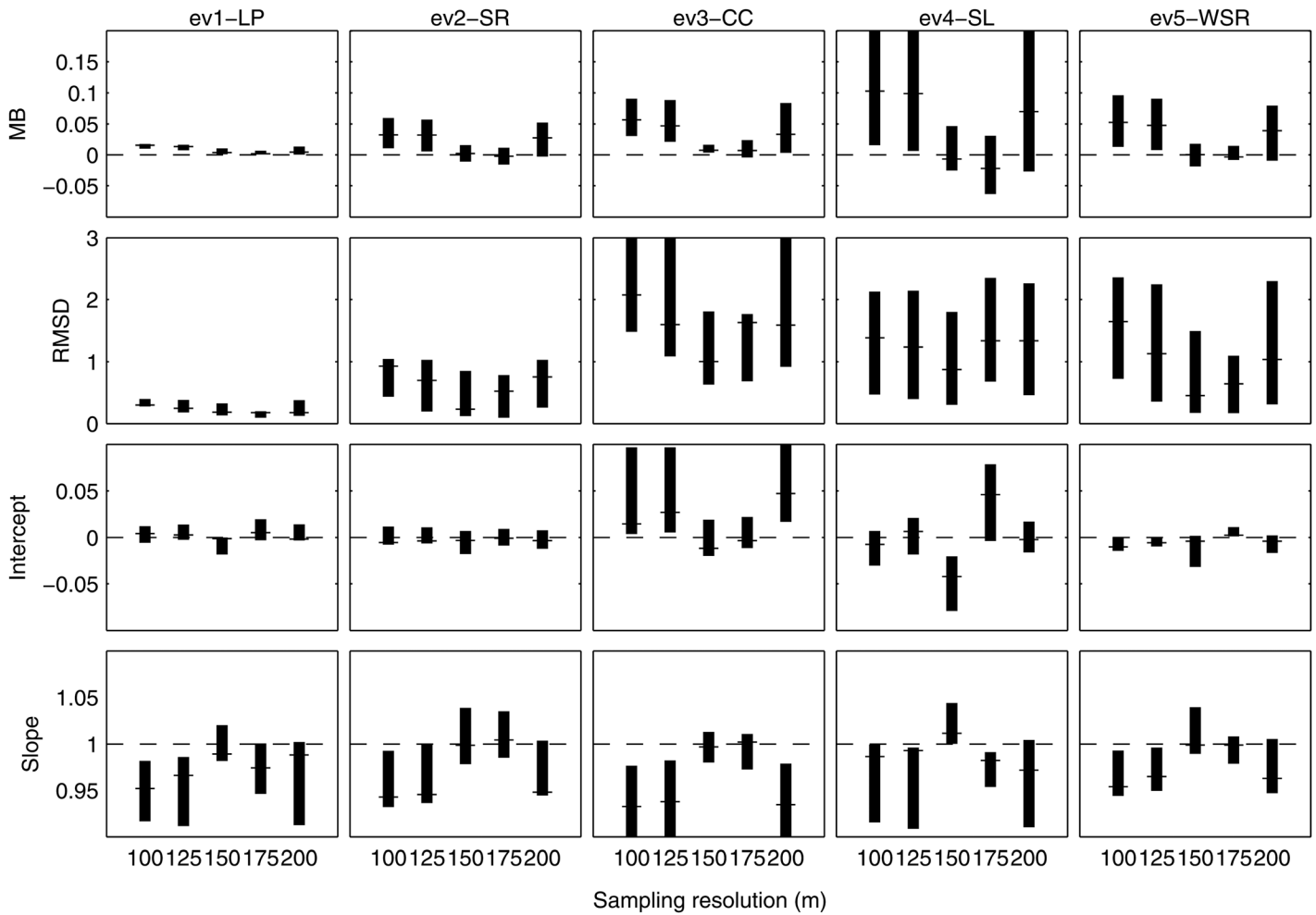
Figure 1. Indicators of the degree of correspondence (Mean Bias (MB), Root-Mean-Squared-Deviation (RMSD), and the intercept and the slope of a linear regression) between radar images sampled in Cartesian and in polar coordinates, as a function of sampling resolution in meters, for the five events under analysis. Boxplots were constructed with ensembles of aggregated radar images for scales ranging from 0.25 to 8 km.

(1) is a deterministic relation at the point (time or space) scale for which stochastic effects due to Drop Size Distribution (DSD) variability can be neglected [*Jaffrain and Berne*, 2012].

In what follows, we consider an ensemble of radar reflectivities Z and the estimator of the mean rain rate $E[R(Z)]$ based on a Taylor expansion of the function $R(Z)$ around $\bar{Z} = E[Z]$:

$$\bar{R} = E[R(Z)] = R(\bar{Z}) \sum_{n=0}^{\infty} \binom{1/b}{n} \frac{E\left[(Z-\bar{Z})^n\right]}{\bar{Z}^n}, \tag{2}$$

where

$$\binom{1/b}{n} = \frac{\Gamma(1+1/b)}{\Gamma(1+1/b-n)\Gamma(1+n)}, \tag{3}$$

and Γ is the gamma function. As $1/b$ is generally noninteger, the Taylor expansion equation (2) converges when fluctuations in the reflectivity field are moderate (i.e., $|Z - E[Z]| < E[Z]$). Retaining the first three terms of the series expansion leads to an expression for the Mean Bias (MB):

$$MB = R(\bar{Z}) - \bar{R} \approx -\frac{1}{2b}\left(\frac{1}{b}-1\right)R(\bar{Z})CV_Z^2, \tag{4}$$

where CV_Z is the coefficient of variation of an ensemble of local or instantaneous radar reflectivities, defined as the ratio between the standard deviation and the mean value. Equation (4) describes the bias due to aggregation and is always positive because $R(Z)$ is a concave function ($b > 1$) in the case of weather radar. An expression for the Fractional Bias (FB) is given by:

$$FB = \frac{R(\bar{Z})}{\bar{R}} - 1 \approx \frac{\frac{1}{2b}\left(1 - \frac{1}{b}\right)CV_Z^2}{1 + \frac{1}{2b}\left(\frac{1}{b} - 1\right)CV_Z^2}.$$

(5)

In the same manner, an expression for the variance of the rain rate can be obtained as follows:

$$Var[R(Z)] = R(\bar{Z})^2 \sum_{n=0}^{\infty} \binom{1/b}{n}\binom{1/b}{n} \frac{\left(E\left[(Z-\bar{Z})^{2n}\right] - \left(E\left[(Z-\bar{Z})^n\right]\right)^2\right)}{\bar{Z}^{2n}} +$$

$$2R(\bar{Z})^2 \sum_{n \leq m} \binom{1/b}{n}\binom{1/b}{m} \frac{\left(E\left[(Z-\bar{Z})^n(Z-\bar{Z})^m\right] - E\left[(Z-\bar{Z})^n\right]E\left[(Z-\bar{Z})^m\right]\right)}{\bar{Z}^n\bar{Z}^m}.$$

(6)

Retaining the first three terms of the series expansion leads to:

$$Var[R(Z)] = \frac{R(\bar{Z})^2 CV_Z^2}{b^2}\left(1 + \gamma_1\left(\frac{1}{b} - 1\right)CV_Z + \frac{(\gamma_2 - 1)}{4}\left(\frac{1}{b} - 1\right)^2 CV_Z^2\right),$$

(7)

where $\gamma_1 = \mu_3/\sigma^3$ is the skewness and $\gamma_2 = \mu_4/\sigma^4 - 3$ is the excess kurtosis of an ensemble of radar reflectivities (μ_n is the n-th moment around the mean and σ is the standard deviation).

Several indicators of the error associated with the aggregation bias can be derived using the approximations above. The Mean Squared Error (MSE) of the estimator $R(\bar{Z})$ is simply computed as MSE $= Var[R(Z)] + MB^2$. The Root Mean Squared Deviation (RMSD) is defined as the square root of the MSE, whereas the coefficient of variation of the RMSD is given by $CV(RMSD) = \sqrt{CV_R^2 + FB^2}$, with $CV_R = \sqrt{Var[R]/\bar{R}^2}$ the coefficient of variation of the rain rate. Both expressions for FB and CV_R are given in an exact manner when an ensemble of radar reflectivities is distributed in a lognormal fashion:

$$FB = (1 + CV_Z^2)^{\frac{1}{2b}\left(1 - \frac{1}{b}\right)} - 1 \approx \frac{(b-1)}{2b^2}CV_Z^2,$$

(8)

$$CV_R = \sqrt{(1 + CV_Z^2)^{\frac{1}{b^2}} - 1} \approx \frac{CV_Z}{b}.$$

(9)

Figure 2 shows FB and CV_R as a function of b and CV_Z, for the exact expression and the second-order Taylor approximation. Both FB and CV_R are stronger functions of CV_Z than of b. The approximation to CV_R based on the Taylor expansion deviates from the exact expression when b increases from 1 to 2. Similarly, the approximation to FB deviates when b decreases from 2 toward unity. Note that when b tends to unity, FB tends to zero, independently of CV_Z. This is to be expected in case of a linear Z-R relation.

3. Bias and Uncertainty in Rainfall Estimates

3.1. Aggregation Bias

Rainfall rates are successively constructed with aggregated reflectivities $R(\bar{Z})$ and compared with the "true" aggregated rainfall rates $\bar{R}$. For each event, the Mean Bias and the Fractional Bias are computed. Also, the standard deviation of Z and of R are computed within the aggregation interval to calculate CV_Z and CV_R, respectively. The resulting time series of coefficients of variation are averaged over the entire event. Figure 3 shows MB, FB, CV_Z, and CV_R as a function of aggregation scale, per event. Event SL shows the highest increase in bias with scale. FB is a strong function of CV_Z. The outcome of equation (8) using $b = 1.73$ and CV_Z, fits the variation of FB with aggregation scale fairly well, showing minor discrepancies between the exact expression and the Taylor approximation. CV_R is a also strong function of CV_Z and the approximation to CV_R with equation (9) fits the variation with scale well, too. Similar conclusions can be reached in the spatial domain (Figure 4), where variations with scale seem to be less dependent on the event under consideration.
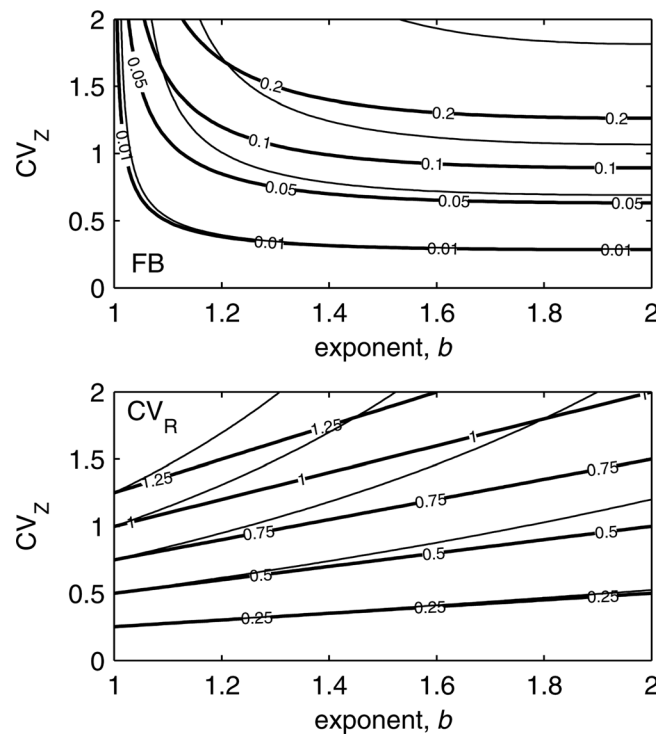
Figure 2. Fractional Bias FB and coefficient of variation of the rain rate CV_R as a function of b and CV_Z, assuming Z is lognormally distributed. Thick lines denote the exact expression, whereas thin lines denote the second-order Taylor approximation.
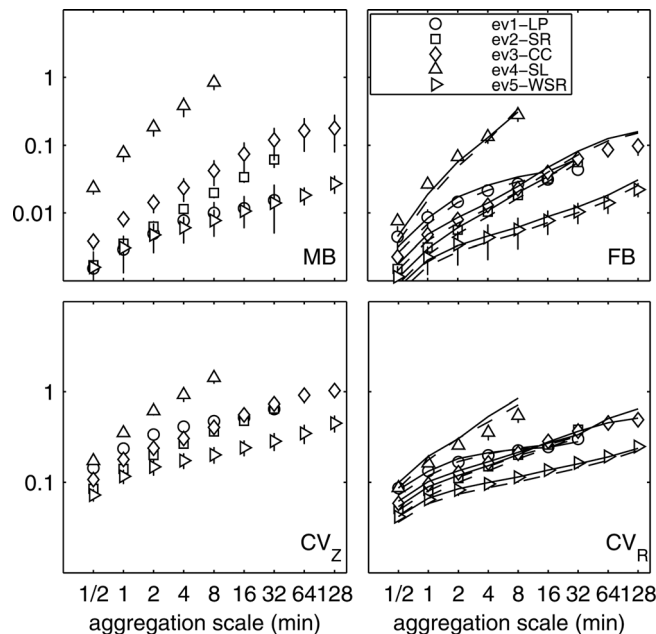

Figure 3. Mean Bias MB, Fractional Bias FB, coefficient of variation of the reflectivity field CV_Z, and coefficient of variation of the rain rate CV_R, as a function of aggregation scale in time, for the five events under analysis. Symbols denote the median of a set of radar pixels, error bars denote the interquartile range. Also shown the outcome of equations (8) and (9) for FB and CV_R, respectively. Dashed lines denote the exact expression whereas solid lines denote the second-order Taylor approximation.

3.2. Uncertainty

To place the aggregation bias into perspective, we compare the RMSD due to aggregation (computed as $\sqrt{\text{Var}[R(Z)] + MB^2}$) with the typical error associated with intermittently sampling the instantaneous rain rate (as operational weather radars do) with a sampling rate set by the aggregation scale. Time series of each radar pixel are divided into ensembles whose length and number are set by the aggregation scale. We compute the RMSD between the ensemble average and the first value of each ensemble; the remaining ensembles are constructed by subsequently sampling the instantaneous rain rate until the last value of the ensemble is reached. This procedure yields an increasing number of RMSD-estimates for increasing scales of aggregation. Finally, we compute the ensemble mean of the RMSD-estimates. The ensemble mean of the RMSD is an indicator of the sampling-related uncertainty as a function of the intermittency level [*Steiner et al.*, 2003]. The RMSD associated with intermittent sampling is generally one order of magnitude larger than the RMSD associated with the aggregation bias (Table 2); however, the former is typically a random error, whereas the latter is systematic and predictable. Moreover, it is important to note that radar Quantitative Precipitation Estimates (QPE) can be corrected for temporal undersampling by assuming space-time coherence of precipitation and by interpolating in time [*Fabry et al.*, 1994], which greatly reduces the sampling uncertainty. Thus, in practice, the magnitude of the predictable component of the error associated with the aggregation bias becomes even more significant.

3.3. Relation to Subgrid Variability
Both FB and CV_R are strongly dependent functions of CV_Z. Aiming to approximate the true, unbiased rain rate and its variance based on aggregated reflectivities, we write FB and CV_R as power functions of CV_Z, $\frac{1}{p}CV_Z^q$, where p and q
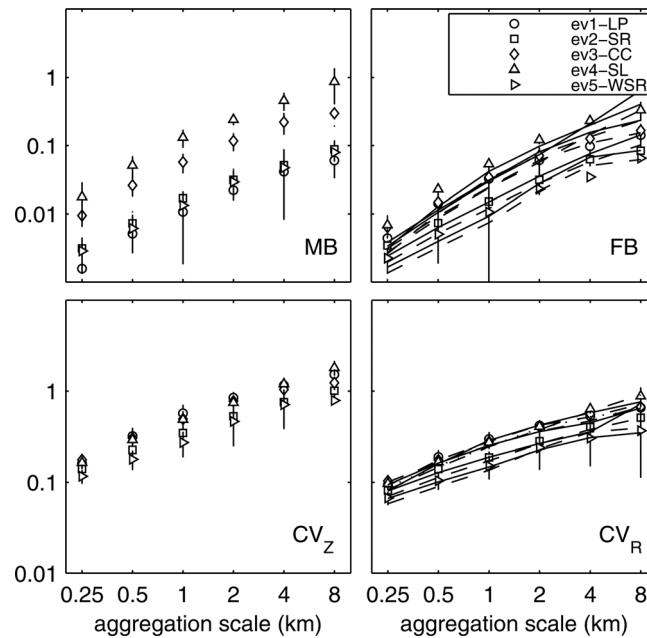
Figure 4. Same as Figure 3, but for spatial aggregation.

denote a prefactor and an exponent, respectively, and are expected to be, respectively, close to 8.2 and 2 for equation (8), and 1.73 (*b*) and 1 for equation (9). Figure 5 shows estimates of *p* and *q* based on linear regression of the log-transformed variables and based on nonlinear regression, for the temporal domain. Both estimates of *p* and *q* in the approximation to CV_R compare fairly well; the means across scales of *p* and *q* yield approximately 1.85 and 0.93, respectively, for both linear and nonlinear regressions. Parameters *p* and *q* show an increase and a decrease with aggregation scale, respectively. The departures show a balancing behavior, which may be related to artifacts of the estimation procedure. In general, good agreement with the expected values mentioned above is found until an aggregation scale of approximately 4 min. Estimates of *p* and *q* in the approx-

imation to FB differ somewhat and show less well-defined scale dependencies. Prefactors estimated with linear and nonlinear regressions are on average about 10 and 8.5, respectively, whereas exponents are on average about 1.5 and 1.7. In the spatial domain (not shown), scale dependencies in *p* and *q* for the approximation to FB are similar to those described above, with the onset of divergence from 8 and 2 (respectively) at an aggregation scale of about 0.5 km. Exponents for the approximation to CV_R estimated with linear and nonlinear regressions show a clear decrease with increasing scale of aggregation. Despite variations with scale, *p* and *q* respectively, are on average about 1.85 and 0.9 in the approximation to CV_R, and on average about 10 and 1.4 in the approximation to FB.

4. Prefactors and Exponents in Aggregated *Z-R* Relations

4.1. Variation With Scale

We consider the parameters *a* and *b* that result from the nonlinear regression between $\bar{R}$ and $\bar{Z}$, for several scales of aggregation in the temporal and spatial domain. In both cases, the rain rate is defined as:

$$R=(Z/a_0)^{1/b_0},\qquad(10)$$

with $a_0=171$ and $b_0=1.73$. The rain rate at successive aggregation scales can be written as:

$$R_s=(Z_s/a_s)^{1/b_s},\qquad(11)$$

where $R_s=\bar{R}$ and $Z_s=\bar{Z}$, both at scale *s*, and a_s and b_s are the scale-dependent prefactor and exponent. By definition, $E[R_s-R]=E[Z_s-Z]=0$, however, $E[(Z_s/a_0)^{1/b_0}-R(Z)] > 0$ when $b_0 > 1$. Equation (11) can be written such that:

$$R_s=\tilde{\alpha}(s)R(\bar{Z})^{\tilde{\beta}(s)},\qquad(12)$$

where $R(\bar{Z})$ is the biased rain rate, and

$$\tilde{\alpha}=f(s)^{-\frac{1}{b_0 g(s)}} \quad \text{and} \quad \tilde{\beta}=g(s)^{-1},\qquad(13)$$

having assumed $a_s/a_0=f(s)$ and $b_s/b_0=g(s)$.

Table 2. Areal Average of the RMSD (mm h^{-1}) Associated With Aggregation (Left Columns) and With Intermittent Sampling (Right Columns) as a Function of Scale, for the Five Events Under Analysis

Scale (min)	ev1-LP		ev2-SR		ev3-CC		ev4-SL		ev5-WSR	
0.5	0.05	0.46	0.05	0.94	0.22	1.59	0.56	4.21	0.09	1.53
1	0.06	0.53	0.07	1.11	0.28	1.91	1.12	5.96	0.10	1.66
2	0.07	0.55	0.08	1.14	0.33	1.93	1.72	7.36	0.11	1.54
4	0.07	0.51	0.10	1.09	0.38	1.83	2.14	7.39	0.09	1.28
8	0.06	0.41	0.11	1.00	0.44	2.00	3.10	6.86	0.07	1.03
16	0.05	0.30	0.13	0.93	0.51	2.04	–	–	0.06	0.83
32	0.04	0.21	0.15	0.83	0.51	2.02	–	–	0.05	0.64
64	–	–	–	–	0.44	1.70	–	–	0.05	0.49
128	–	–	–	–	0.36	1.27	–	–	0.05	0.43

Figure 6 shows the median and the interquartile range of a_s and b_s computed from a set of radar pixels, as a function of aggregation scale. For temporal aggregation, a_s and b_s generally diverge from the values at the finest scale for scales greater than 1–2 min, and exhibit significant variation among events. Event SL has the greatest scale dependency in exponents and prefactors as this type of rainfall typically displays the largest variability and intermittency, both in space and time. Note that the interquartile range of a_s and b_s at a given scale grows with scale and displays a positive correlation with the divergence rate of a given event. For spatial aggregation, both a_s and b_s show similar patterns as for temporal aggregation; however, the interquartile range increases with aggregation scale and is much greater than in the temporal domain. The onset of divergence occurs at an aggregation scale of about 0.5 km for both a_s and b_s. The variation of a_s and b_s with scale shows an ambiguous functional dependence, as transforming the vertical axis in Figure 6 to a logarithmic scale does not necessarily result in either a_s or b_s following straight lines.

4.2. Scaling Functions
We investigate the variation of a_s and b_s with scale by, respectively, proposing three different functional dependencies:

$$f(s)=\left(\frac{s}{s_0}\right)^{\gamma_a}, \quad g(s)=\left(\frac{s}{s_0}\right)^{\gamma_b}, \tag{14}$$

$$f(s)=\exp\left(\gamma_a\frac{s-s_0}{s_0}\right), \quad g(s)=\exp\left(\gamma_b\frac{s-s_0}{s_0}\right), \tag{15}$$

$$f(s)=1+\frac{\gamma_a}{a_0}\left(\frac{s}{s_0}-1\right), \quad g(s)=1+\frac{\gamma_b}{b_0}\left(\frac{s}{s_0}-1\right), \tag{16}$$

where γ is a parameter characterizing how fast the prefactor and exponent diverge with aggregation scale, the subscript 0 denotes the prefactor and exponent at the finest scale, and the subscript s denotes the prefactor and exponent at scale s. For each proposed scaling function, we force the fit at the origin (assuming known a_0 and b_0) and we allow a break in scaling by matching the two functions in linear or logarithmic space [*Guo*, 2002; *Sassi et al.*, 2012b], where applicable. The location of the break in scaling obtained with the three models proposed above, for the temporal and spatial domain, is shown in Figure 7. The power law consistently yields a lower value than the exponential and linear models, which generally agree. The break in scaling in the time domain is event-dependent (about 2 min for SL, 4 min for LP and SR, and 8 min for CC and WSR), but shows a remarkable consistency in the spatial domain (about 1.5 km for all events).

In what follows, we select the results from the power-law fit because: the power-law fit yields less variability in the estimated parameters, as shown by the size of the boxes in Figure 7; the power-law fit yields the lowest standard error normalized by the parameter (not shown); and the power-law fit allows us to compare and discuss our results in the framework presented by *Verrier et al.* [2013]. Note the exponential and linear model qualitatively show the same results (albeit with different γ values), which is readily explained because the linear model represents the first two terms of the Taylor series expansion of the exponential model. Statistical measures of the goodness-of-fit such as the coefficient of determination did not help in deciding which model performs best.

Both the prefactor and the exponent grow more rapidly with scale in the temporal domain for events LP and SL (Figure 8). For the prefactor a_s, the ratio of the absolute value of the exponent in the upper scaling regime (denoted with $\gamma_{a,hi}$) to the absolute value of the exponent in the lower scaling regime (denoted with
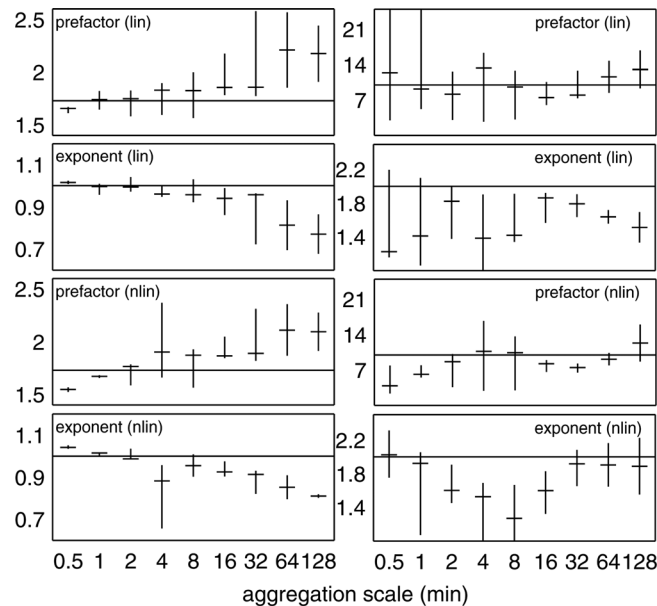
Figure 5. Exponent and prefactor in equation (8) (right) and equation (9) (left) for linear (lin) and nonlinear (nlin) regression, as a function of aggregation scale in time. Boxplots are constructed based on estimates for each event. Solid lines denote the values expected from the corresponding equations.

$\gamma_{a,lo}$) remains relatively constant across events (the mean of the medians is about 2). For the exponent b_s, this ratio shows more variability between and within (particularly SR and CC) events, with an overall mean of the medians of about 3.5. Overall, absolute values of γ_a and the ratio of $\gamma_{a,hi}$ to $\gamma_{a,lo}$ are in good agreement with the values reported in the literature (see Table 1 in *Verrier et al.* [2013]). In the spatial domain (Figure 9), the rate of divergence of the prefactor for the five events shows the same behavior as in the temporal domain, whereas $\gamma_{b,lo}$ shows more uniformity across events. The ratio of γ_{hi} to γ_{lo} remains relatively constant for both prefactor and exponent, with an overall mean of the medians of about 1.5.

5. Variability of Radar Reflectivities

The previous sections showed the aggregation bias can be constrained if the coefficient of variation of the reflectivity field at the subgrid scale is known, and that the scaling of the prefactor and the exponent in *Z-R* relations of aggregated variables may be represented with prescribed functions. Here we present several descriptors of variability of the reflectivity field in the temporal and spatial domain and discuss these descriptors in light of the previous results.

5.1. Moment Scaling Functions

We have shown previously that γ arises as a consequence of the bias due to aggregation and that this bias can be approximated with the coefficient of variation of the reflectivity field CV_Z. In a multifractal context, *Verrier et al.* [2013] showed that the mean bias due to aggregation can be approximated with a scaling term depending on $K(1/b_0 \sim 0.58)$, with K the moment scaling function of the reflectivity field. Attempting to link the empirically derived γ's with known descriptors of variability, we determine the moment scaling function. The moment scaling function $K(q)$ can be determined empirically by calculating the q-th order moments as a function of aggregation scale and obtaining the slope in log-log plots between these two. Theoretically, the moment scaling function is such that $K(0)=K(1)=0$, $K(q)<0$ for $0<q<1$, and $K(q)>0$ for $q>1$, where q denotes the order of the moment. Determining $K(q)$ empirically in the time
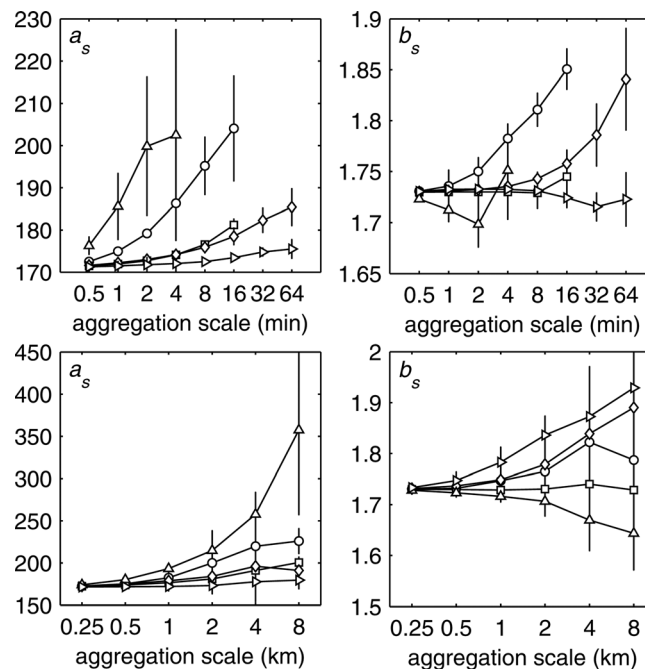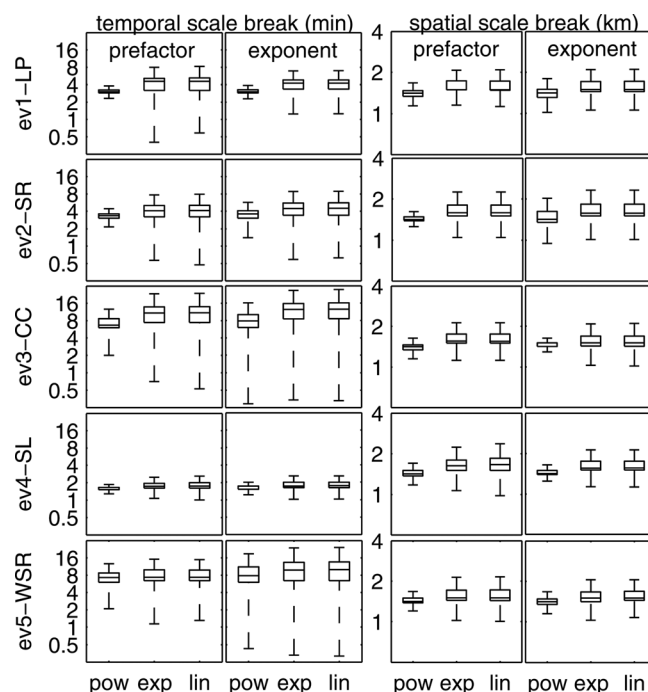

Figure 6. Prefactor a_s and exponent b_s in *Z-R* relations, as a function of aggregation scale in time (top) and in space (bottom), for the five events under analysis. Symbols denote the median of a set of radar pixels, error bars denote the interquartile range, (circle) LP, (square) SR, (diamond) CC, (triangle) SL, and (right-pointing triangle) WSR.

Figure 7. Location of the break in temporal (left) and spatial (right) scaling in the prefactor and the exponent, for the five events under analysis, estimated with the power (pow), exponential (exp), and linear (lin) models. Boxplots are constructed based on a set of radar pixels.

domain poses several difficulties such as intermittency bias [e.g., *de Montera et al.*, 2009; *Gires et al.*, 2012] and sensitivity to higher-order moments [*Lombardo et al.*, 2014].

Following the methods described in *de Montera et al.* [2009], we determine K for moments with order q ranging from 0.2 to 2 in steps of 0.2, for each radar pixel and event and using the same range of scales of aggregation as before. Noting that $CV_Z^2 + 1 = \langle Z_s^2 \rangle / \langle Z_s \rangle^2$, we investigate the relation of γ with $K(2) - 2K(1)$ [*Venugopal et al.*, 2006]. Note that $K(1)$ is theoretically zero but due to numerical artifacts of the regression procedure it may deviate slightly from zero. The quality of the scaling behavior has been assessed with the coefficient of determination R^2, which is a measure of the goodness-of-fit of the linear regression between the log-transformed variables. Most of the R^2-values are significantly greater than 0.5, except for q close to 1

(where the slope is nearly zero). Figure 10 shows density plots of $K(2) - 2K(1)$ (and $-K(0.6)$) and γ_{lo}, for the prefactor a_s and the exponent b_s, respectively. It is evident that the correspondence of the two descriptors with $\gamma_{a,lo}$ is greater than with $\gamma_{b,lo}$, both within and among events. The discrepancies between descriptors may arise due to the limitations of the present approach, such as the possible lack of convergence of the

Figure 8. Summary of exponents γ obtained with the power-law fit in the temporal domain for prefactor (left, subscript a) and exponent (right, subscript b), for the five events under analysis. Values obtained below the break are denoted with the subscript lo, whereas values above the break with the subscript hi. Boxplots are constructed based on a set of radar pixels and represent the first, second, and third quartile. Exponents presented here correspond to the absolute value.

Taylor expansion and the truncation of such series at moments of order two. Nevertheless, even for cases where the Taylor expansion does not converge ($CV_Z > 1$), it performs reasonably well compared to the exact solution for the strongly fluctuating lognormal case (see Figure 2).

5.2. Structural Analysis
The spatial analysis of statistical moments with aggregation scale based on the multifractal formalism posses the same difficulties as in the time domain [*Verrier et al.*, 2010]. Spatial rainfall based on C-band radar data shows scaling regimes characterized by breaks [e.g., *Tessier et al.*, 1993; *Verrier et al.*, 2013]; however, at higher spatial resolutions, the determination of $K(q)$ may be severely affected by intermittency bias [e.g., *Schmitt et al.*, 1998; *Gires et al.*, 2012, 2013] and the stochastic variability of the drop-size
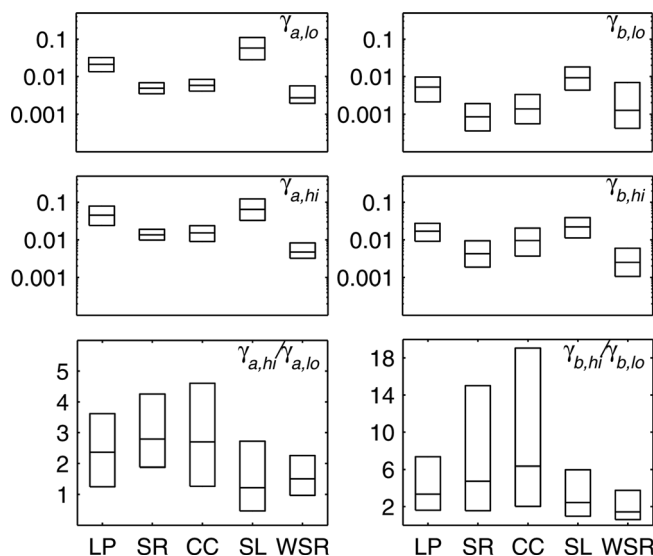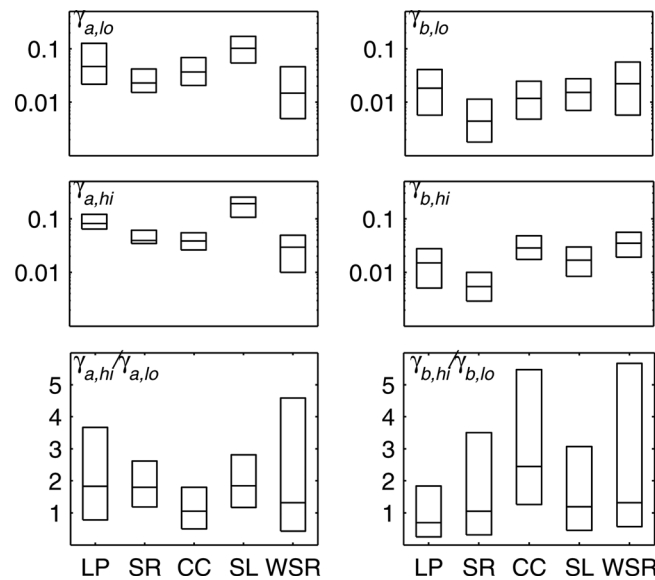
Figure 9. Same as Figure 8, but for spatial aggregation.

distribution [*Jaffrain and Berne*, 2012]. Here we adopt an alternative approach to investigate the relation between spatial variability and aggregation bias.

We compute the generalized isotropic variogram of order q [*Lavallée et al.*, 1993; *Rodriguez-Iturbe and Rinaldo*, 1997]:

$$\hat{C}_q(h) = \langle |Z(r) - Z(r+h)|^q \rangle = \langle |\Delta Z(h)|^q \rangle, \tag{17}$$

where the brackets denote averaging over all pairs separated by the lag distance h, for q ranging from 0.2 to 2 in steps of 0.2, and h in the range 0–20 km. Since the analysis may be sensitive to the discretization of the spatial lag h employed in constructing the variograms, we use a resolution of 250 m (the smallest aggregation scale). We generate 100 realizations of $\hat{C}_q(h)$ by shuffling the sampled locations using a uniformly distributed random generator (300 "wet" points defined as $Z > 10$ dBZ, which corresponds to the lowest rain rates), we then retain the ensemble median, and normalize the latter with the area under the curve, to yield a robust estimate of the q-th order normalized variogram $C_q(h)$. The procedure is applied to data aggregated in space using the scales of aggregation from 0.25 to 8 km. Results are then resampled at the highest resolution (0.25 km) to allow regression on each pixel. Figure 11 gives an impression of $C_{q,s}(h)$ for various q- and s-values, for the event LP. Most commonly used nugget-free variogram models in traditional experimental semivariogram analysis may be represented by two shape factors that are equivalent to the range and sill of e.g., exponential and spherical variograms [*Van de Beek et al.*, 2011]. The sill is the limit of the variogram whereas the range is the distance at which the difference of the variogram from the sill becomes negligible. Note that the sill corresponds to the normalized sill (by the total area under the curve). The increase in range that is observed in all variograms is a direct consequence of aggregation [*Berne et al.*, 2004]; also the shape of the variogram becomes increasingly more curved with aggregation, thus affecting the determination of the shape factors.

We parameterize $C_{q,s}(h)$ by fitting a bounded bilinear and an unbounded exponential variogram model with zero nugget, respectively, to yield a set of two shape factors (corresponding to the range and the normalized sill), both functions of the order of the moment q and aggregation scale s. Log-log plots of the shape factors against s clearly show a break at $s = 1$–2 km (not shown). Power-law scaling in variogram shape parameters is commonly found in seasonal semivariance analysis [e.g., *Van de Beek et al.*, 2012]. Therefore, for each shape factor, we fit a power function of s and we allow for a break by matching the two functions. The procedure is performed with each image to yield a set of scaling exponents as a function of q, per event. We then calculate the medians of the exponents and the locations of the break over the entire event. The median exponents in the lower regime and the median location of the break are plotted against q in Figure 12. Both scaling functions of the range and the normalized sill are nonlinear. Exponents of the normalized sill are nearly zero, confirming the limited dependence of this shape parameter on aggregation scale (note the inconsistent variation with q among events). Exponents of the range clearly show a strong dependence on aggregation scale, in particular for moments of order $q < 1$. The bounded and unbounded models result in similar shapes of the scaling functions, tough the unbounded model shows a more rapid decrease with q. The location of the break is nearly constant for all values of q and is on average about 1.4 km for all events, with the WSR event showing slightly lower values. These results are consistent with the location of the break of the prefactor and exponent in aggregated Z-R relations, shown in Figure 7.
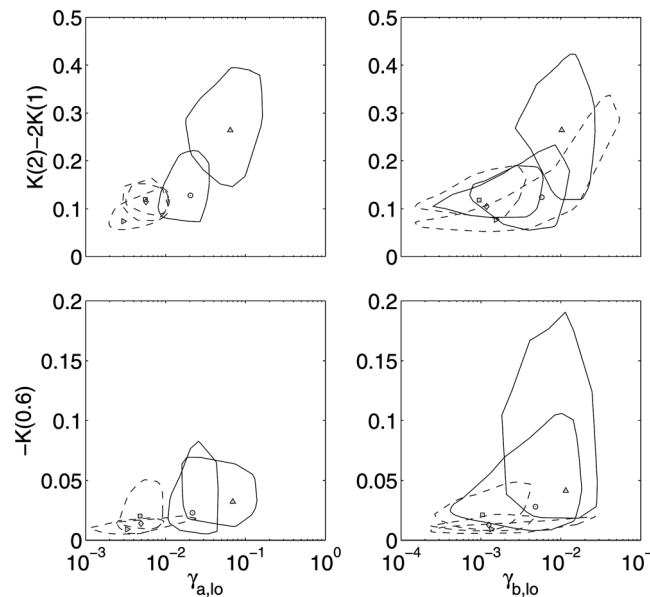
Figure 10. Density plots of $K(2)-2K(1)$ (top) and $-K(0.6)$ (bottom) and γ, for the prefactor ($\gamma_{a,lo}$) and the exponent ($\gamma_{b,lo}$), respectively, for the five events under analysis. Symbols denote the observations with highest density, (circle) LP, (square) SR, (diamond) CC, (triangle) SL, and (right-pointing triangle) WSR, lines denote the bag containing half of the observations with largest density. Lines are drawn with different styles for visualization purposes only.

6. Discussion

Results obtained with nonlinear regression indicate both prefactor and exponents in aggregated *Z-R* relations suffer a dependency with scale that is summarized with the exponents γ_a and γ_b, respectively. In the analysis of time series of disdrometer data and employing nonlinear regression, *Verrier et al.* [2013] found only γ_a to be correlated with the moment scaling function. In particular, they suggest that in practice the actual values can differ because the exponent in aggregated *Z-R* relations may be sensitive to the regression procedure. To test the hypothesis that regression may introduce spurious scale dependencies, we performed the analysis carried out in section 4 by fixing the exponent *b* to 1.73. Figure 13 shows that for events SR and WSR, the scale dependencies are practically insensitive to the regression procedure throughout the scales of aggregation considered here; this is also confirmed by the limited scale dependency b_s shows in Figure 6.

Large discrepancies in the estimated prefactors arise for events LP, CC, and SL; however, the discrepancies in the cost functions (denoted by the RMSD of the residuals) are mostly evident in the upper scaling regime (scale break is located at about 2–8 min, depending on the event). The same analysis in the spatial domain (not shown) yields similar results with only event SR showing limited sensitivity to the regression procedure; in all other cases, discrepancies in cost functions arise for scales of aggregation above 1 km. Our results confirm that the scale dependency of b_s may be an artifact of the regression procedure. Since aggregation introduces a bias that is a function of *Z*, log-log plots of *Z* versus *R* will exhibit less scatter for large *Z* and this effectively translates into variation in the exponent. Based on the fact that there is a linear relation between the true aggregated *R* and the rainfall intensity estimated from the aggregated *Z* (see equation (2)), we indeed expect only the prefactor of the power function to be affected by scale [*Verrier et al.*, 2013].

The structural analysis employing *q*-th order generalized variograms showed the scaling properties of shape parameters remain qualitatively comparable for bounded and unbounded variogram models and that the range seems to be insensitive to the scale of aggregation for $q > 1$. The coefficient of variation of *Z*, however, shows a strong dependence on aggregation for scales up to 8 km (see Figure 4). Without parameterizing the variogram, any *q*-th order variogram is said to be scaling if [*Lavallée et al.*, 1993; *Rodriguez-Iturbe and Rinaldo*, 1997]

$$C_{q,s}(h) \sim s^{-\zeta(q,h)}, \tag{18}$$

where *h* is the spatial resolution of the variogram, *s* denotes the aggregation scale, and $\zeta(q,h)$ is the structure function exponent, which is estimated independently for each individual *h*. The ratio

$$\frac{C_{2,s}^{1/2}}{C_{1,s}} = \frac{\sqrt{\langle|\Delta Z_s(h)|^2\rangle}}{\langle|\Delta Z_s(h)|\rangle} \sim s^{-\frac{\zeta(2,h)}{2}+\zeta(1,h)}, \tag{19}$$

is adopted here as a descriptor of the range-dependent coefficient of variation of the differences, having assumed an isotropic field. Figure 14 shows the exponent in equation (19) as a function of the spatial lag *h*, for the five events under analysis. Up to spatial lags ranging from 3 to 7 km, depending on the event, the
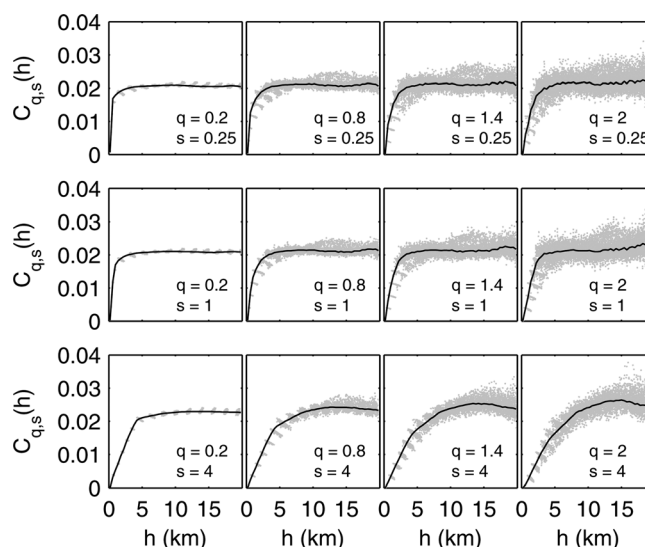
Figure 11. Normalized q-th order variogram $C_{q,s}(h)$ for various values of q and s (km), for the event LP. Gray-dotted lines denote temporal fluctuations, whereas black solid lines denote the median over the entire event.

coefficient of variation of the differences increases with scale, as $-\frac{\zeta(2)}{2}+\zeta(1)$ remains strictly positive, in accordance with previous results. For greater spatial lags, the coefficient of variation of the differences decreases with aggregation scale. This result is consistent with observations of spatial rainfall with satellites [e.g., *Gupta and Waymire*, 1990; *Olsson et al.*, 1999], that exhibit monotonically decreasing moment scaling functions for moments higher than unity. Note that the direct analysis of variability carried out with CV_Z at large scales of aggregation may be severely hampered by the limited spatial coverage of the X-band radar. The structural analysis could constitute a possible alternative of analysis if the results complement those of the traditional approach; however, if the range of the variograms is larger than the domain covered by the radar, the structural analysis will be equally affected.

Throughout our analysis, we have neglected the correction for attenuation of the radar signal along its path. Attenuation in the X-band is known to be severe for ranges larger than 10 km and mean rain rates exceeding 10 mm h^{-1} [*Uijlenhoet and Berne*, 2008]. For the typical range and rain rates in this study, the possibility of a systematic bias due to attenuation that may affect the conclusions of our spatial analysis is limited. Moreover, the exponent in power functions of attenuation versus rain rate (known as k-R relations) is typically closer to unity [e.g., *Berne and Uijlenhoet*, 2007] than the exponent in Z-R relations, so that the bias due to aggregation in attenuation may be better constrained than the bias in reflectivity. It is interesting that the more linear character of k-R relations may help in better constraining the errors introduced by the inherent point-scale calibration of path integrated attenuations measured by microwave links [*Berne and Uijlenhoet*, 2007; *Leijnse et al.*, 2008, 2010; *Overeem et al.*, 2011]. A further direction of investigation may include a sensitivity analysis to reveal under which conditions power functions such as Z-R and k-R relations exhibit a weakly nonlinear character. This sensitivity analysis may be based on a multivariate Taylor series expansion of equation (1).

The results of our analysis clearly support the possibility, and urge the necessity, to attach ranges of validity to nonlinear calibrations. *Marshall* [1969] was among the first to recognize that radar calibration intrinsically requires a scale-dependent reference range to overcome the difficulties of inhomogeneous Z-R relations. Particularly, here we show nonlinear calibrations are susceptible to systematic aggregation bias and that the bias is very much associated with the variability of the quantity we are interested in. Radars provide an excellent trade-off between spatial and temporal resolution (and coverage) that allows us to investigate the rainfall variability at several scales and possibly constrain the aggregation bias. In other fields involving remote sensing of environmental
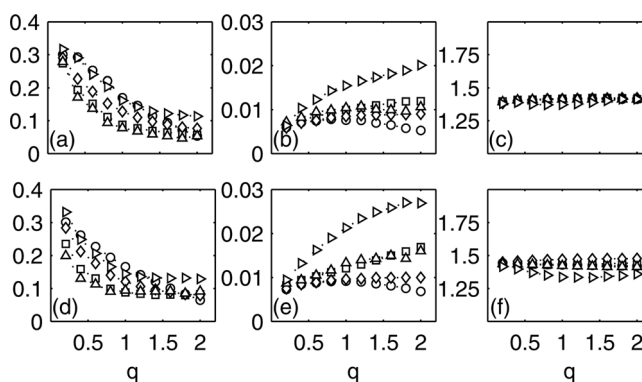

Figure 12. Scaling function of the shape factors of q-th order generalized variograms for the bilinear (a and b, range and normalized sill, respectively) and exponential models (d and e, range and normalized sill, respectively), for the five events under analysis, (circle) LP, (square) SR, (diamond) CC, (triangle) SL, and (right-pointing triangle) WSR. (c) and (f) show the location of the break (km) of the range and normalized sill with s.
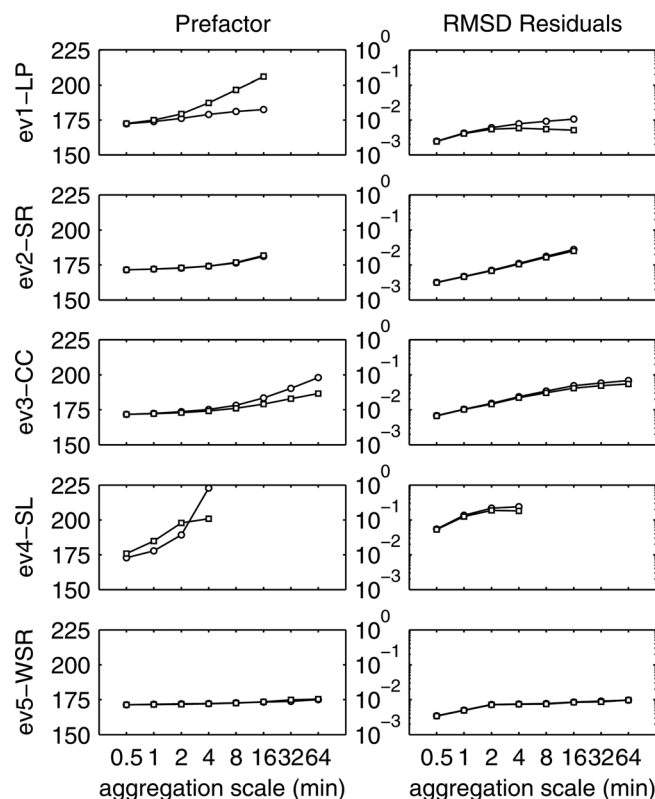
Figure 13. (left) Prefactor a_s obtained with nonlinear regression keeping b constant (circles) and free (squares) as a function of aggregation scale in time, for the five events under analysis. (right) RMSD of the residuals.

observables (e.g., sediment transport, [*Sassi et al.*, 2012a]), however, one first has to overcome methodological complications in order to address the problem of aggregation. Therefore, being cautious about the range of validity of a certain calibration or empirically-derived formula is even more stringent.

7. Summary and Conclusions

Rain radars routinely rely on power functions to retrieve rain rates based on radar reflectivities measured at widely ranging spatial and temporal resolutions. The nonlinear nature of power functions may complicate the comparison of rainfall estimates employing reflectivities measured at different scales, as transforming reflectivity Z into rain rate R using relations that have been derived for other spatial and/or temporal scales results in a bias. Here we investigated the sensitivity of such power functions, known as Z-R relations, to spatial and temporal aggregation using high-resolution reflectivity fields measured with an X-band radar, for five

rainfall events. Existing Z-R relations were employed to investigate the behavior of aggregated Z-R relations with scale, the aggregation bias, and the variability of the estimated rain rate. An approximation of the mean rain rate based on a Taylor expansion allowed us to derive expressions for the bias and the variability of the estimated rain rate, both strong functions of the coefficient of the subgrid-scale variation of the reflectivity CV_Z.

The prefactor and the exponent of aggregated Z-R relations systematically diverge with scale, showing breaks that are event-dependent in the temporal domain and nearly constant in the spatial domain. The systematic behavior of prefactors and exponents with scale can be described with prescribed functions, notably power, linear, and exponential functions. The systematic error a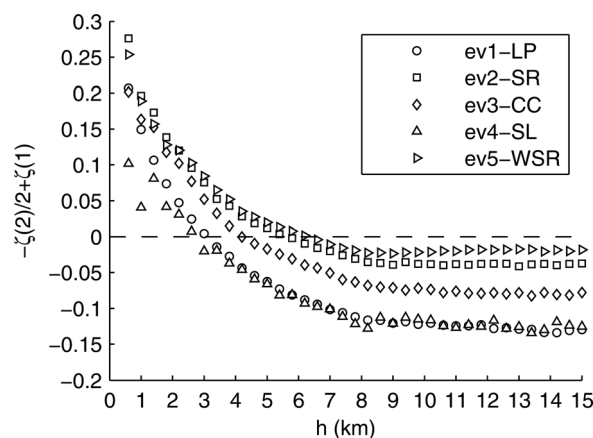ssociated with aggregation bias at a given scale can be of the same order of magnitude as the corresponding random error associated with intermittent sampling. The predictable bias can be easily constrained by including information about the variability of Z within a certain scale of aggregation, and is captured by simple functions of CV_Z. Several descriptors of spatial and temporal variability of the reflectivity field show strong links with aggregation bias. Prefactors in Z-R relations can be related to multifractal properties of the rainfall field, whereas scale dependencies in the exponent may be interpreted as a spurious artifact of the regression procedure. Shape factors of both bounded bilinear and unbounded exponential variogram models are insensitive to aggregation for moments of

Figure 14. Structure function exponent in equation (19) as a function of the spatial lag h, for the five events under analysis.

order higher than unity; however, the structural analysis of spatial rainfall reveals a scaling break at spatial lags comparable with the maximum scale of aggregation imposed by the limited spatial coverage of the radar data set analyzed. Our results support the good practice of attaching ranges of validity to nonlinear calibrations.

References

Battan, L. J. (1973), *Radar Observation of the Atmosphere*, 324 pp., Univ. of Chicago Press, Chicago, Ill.

Berne, A., and R. Uijlenhoet (2007), Path-averaged rainfall estimation using microwave links: Uncertainty due to spatial rainfall variability, *Geophys. Res. Lett.*, *34*, L07403, doi:10.1029/2007GL029409.

Berne, A., G. Delrieu, J. Creutin, and C. Obled (2004), Temporal and spatial resolution of rainfall measurements required for urban hydrology, *J. Hydrol.*, *3–4*, 166–179.

de Montera, L., L. Barthès, C. Mallet, and P. Golé (2009), The effect of rain-no rain intermittency on the estimation of the universal multifractals model parameters, *J. Hydrometeorol.*, *10*(2), 493–506.

Fabry, F. (1996), On the determination of scale ranges for precipitation fields, *J. Geophys. Res.*, *101*(D8), 819–826, doi:10.1029/96JD00718.

Fabry, F., A. Bellon, M. R. Duncan, and G. L. Austin (1994), High resolution rainfall measurements by radar for very small basins: The sampling problem reexamined, *J. Hydrol.*, *161*(1–4), 415–428.

Ferguson, R. I. (2003), The missing dimension: Effects of lateral variation on 1-D calculations of fluvial bedload transport, *Geomorphology*, *56*(1–2), 1–14.

Gires, A., I. Tchiguirinskaia, D. Schertzer, and S. Lovejoy (2012), Influence of the zero-rainfall on the assessment of the multifractal parameters, *Adv. Water Resour.*, *45*, 13–25.

Gires, A., I. Tchiguirinskaia, D. Schertzer, and S. Lovejoy (2013), Development and analysis of a simple model to represent the zero rainfall in a universal multifractal framework, *Nonlinear Process. Geophys.*, *20*, 343–356.

Guo, J. (2002), Logarithmic matching and its applications in computational hydraulics and sediment transport, *J. Hydraul. Res.*, *40*(5), 555–565.

Gupta, V. K., and E. Waymire (1990), Multiscaling properties of spatial rainfall and river flow distributions, *J. Geophys. Res.*, *95*(D3), 1999–2009, doi:10.1029/JD095iD03p01999.

Heuvelink, G. B. M., and E. J. Pebesma (2009), Spatial aggregation and soil process modelling, *Geoderma*, *99*(1–2), 47–65.

Jaffrain, J., and A. Berne (2012), Influence of the subgrid variability of the raindrop size distribution on radar rainfall estimators, *J. Appl. Meteorol.*, *51*(4), 780–785.

Lavallée, D., S. Lovejoy, D. Schertzer, and P. Ladoy (1993), Nonlinear variability of landscape topography: Multifractal analysis and simulation, chap., in *Fractals in Geography*, pp. 158–192, Prentice Hall, Englewood Cliffs, N. J.

Leijnse, H., R. Uijlenhoet, and J. N. M. Stricker (2007a), Rainfall measurement using radio links from cellular communication networks, *Water Resour. Res.*, *43*, W03201, doi:10.1029/2006WR005631.

Leijnse, H., R. Uijlenhoet, and J. N. M. Stricker (2007b), Hydrometeorological application of a microwave link: 2. Precipitation, *Water Resour. Res.*, *43*, W04417, doi:10.1029/2006WR004989.

Leijnse, H., R. Uijlenhoet, and J. N. M. Stricker (2008), Microwave link rainfall estimation: Effects of link length and frequency, temporal sampling, power resolution, and wet antenna attenuation, *Adv. Water Resour.*, *31*(11), 1481–1493.

Leijnse, H., R. Uijlenhoet, and A. Berne (2010), Errors and uncertainties in microwave link rainfall estimation explored using drop size measurements and high-resolution radar data, *J. Hydrometeorol.*, *11*, 1330–1344.

Ligthart, L. P., and L. R. Nieuwkerk (1990), An X-band solid-state FM-CW weather radar, *IEE Proc. F Radar Signal Process.*, *137*(6), 418–426.

Lombardo, F., E. Volpi, D. Koutsoyiannis, and S. M. Papalexiou (2014), Just two moments! A cautionary note against use of high-order moments in multifractal models in hydrology, *Hydrol. Earth Syst. Sci.*, *18*, 243–255.

Lovejoy, S., and D. Schertzer (1990), Fractals, raindrops and resolution dependence of rain measurements, *J. Appl. Meteorol.*, *29*(11), 1167–1170.

Mandapaka, P. V., P. Lewandowski, W. E. Eichinger, and W. F. Krajewski (2009), Multiscaling analysis of high resolution space-time lidar-rainfall, *Nonlinear Process. Geophys.*, *16*, 579–586.

Marani, M. (2005), Non-power-law scale properties of rainfall in space and time, *Water Resour. Res.*, *41*, W08413, doi:10.1029/2004WR003822.

Marshall, J. S. (1969), Power-law relations in radar meteorology, *J. Appl. Meteorol.*, *8*, 171–172.

Mascaro, G., R. Deidda, and M. Hellies (2013), On the nature of rainfall intermittency as revealed by different metrics and sampling approaches, *Hydrol. Earth Syst. Sci.*, *17*, 355–369.

Miller, D. M. (1984), Reducing transformation bias in curve fitting, *Am. Stat.*, *38*(2), 124–126.

Moglen, G. E., and G. L. Hartman (2001), Resolution effects on hydrologic modeling parameters and peak discharge, *J. Hydrol. Eng.*, *6*(6), 490–497.

Nykanen, D., and E. Foufoula-Georgiou (2001), Soil moisture variability and its effect on scale-dependency of nonlinear parameterizations in coupled land-atmosphere models, *Adv. Water Resour.*, *24*(9–10), 1143–1157.

Olsson, J., V. P. Singh, and K. Jinno (1999), Effect of spatial averaging on temporal statistical and scaling properties of rainfall, *J. Geophys. Res.*, *104*(D16), 19,117–19,126, doi:10.1029/1999JD900271.

Overeem, A., H. Leijnse, and R. Uijlenhoet (2011), Measuring urban rainfall using microwave links from commercial cellular communication networks, *Water Resour. Res.*, *47*, W12505, doi:10.1029/2010WR010350.

Recking, A. (2013), An analysis of nonlinearity effects on bed load transport prediction, *J. Geophys. Res. Earth Surf.*, *118*, 1264–1281, doi:10.1002/jgrf.20090.

Rodriguez-Iturbe, I., and A. Rinaldo (1997), *Fractal River Basins: Chance and Self-Organization*, Cambridge University Press, Cambridge, U. K.

Sassi, M., A. Hoitink, and B. Vermeulen (2012a), Impact of sound attenuation by suspended sediment on ADCP backscatter calibrations, *Water Resour. Res.*, *48*, W09520, doi:10.1029/2012WR012008. Physical Oceanography, Den Burg, Texel., Netherlands.

Sassi, M., A. Hoitink, B. de Brye, and E. Deleersnijder (2012b), Downstream hydraulic geometry of a tidally influenced river delta, *J. Geophys. Res.*, *117*, F04022, doi:10.1029/2012JF002448.

Schertzer, D., and S. Lovejoy (1987), Physical modeling and analysis of rain and clouds by anisotropic scaling multiplicative processes, *J. Geophys. Res.*, *92*(D8), 9693–9714, doi:10.1029/JD092iD08p09693.

Schmitt, F., S. Vannitsem, and A. Barbosa (1998), Modeling of rainfall time series using two-state renewal processes and multifractals, *J. Geophys. Res.*, *103*(D18), 23,181–23,193, doi:10.1029/98JD02071.

Smith, J. A., and W. F. Krajewski (1993), A modeling study of rainfall rate-reflectivity relationships, *Water Resour. Res.*, *29*(8), 2505–2514, doi: 10.1029/93WR00962.

Steiner, M., and J. A. Smith (2004), Scale dependence of radar-rainfall rates An assessment based on raindrop spectra, *J. Hydrometeorol.*, *5*(6), 1171–1180.

Steiner, M., T. L. Bell, Y. Zhang, and E. F. Wood (2003), Comparison of two methods for estimating the sampling-related uncertainty of satellite rainfall averages based on a large radar dataset, *J. Clim.*, *16*(22), 3759–3778.

Tessier, Y., S. Lovejoy, and D. Schertzer (1993), Universal multifractals: Theory and observations for rain and clouds, *J. Appl. Meteorol.*, *32*(2), 223–250.

Uijlenhoet, R. (2001), Raindrop size distributions and radar reflectivity-rain rate relationships for radar hydrology, *Hydrol. Earth Syst. Sci.*, *5*(4), 615–627.

Uijlenhoet, R., and A. Berne (2008), Stochastic simulation experiment to assess radar rainfall retrieval uncertainties associated with attenuation and its correction, *Hydrol. Earth Syst. Sci.*, *12*(2), 587–601.

Uijlenhoet, R., J. Cohard, and M. Gosset (2011), Path-average rainfall estimation from optical extinction measurements using a large-aperture scintillometer, *J. Hydrometeorol.*, *12*(5), 955–972.

Van de Beek, C. Z., H. Leijnse, J. N. M. Stricker, R. Uijlenhoet, and H. W. J. Russchenberg (2010), Performance of high-resolution X-band radar for rainfall measurement in The Netherlands, *Hydrol. Earth Syst. Sci.*, *14*(2), 205–221.

Van de Beek, C. Z., H. Leijnse, P. J. J. F. Torfs, and R. Uijlenhoet (2011), Climatology of daily rainfall semi-variance in the Netherlands, *Hydrol. Earth Syst. Sci.*, *15*(1), 171–183.

Van de Beek, C. Z., H. Leijnse, P. J. J. F. Torfs, and R. Uijlenhoet (2012), Seasonal semi-variance of Dutch rainfall at hourly to daily scales, *Adv. Water Resour.*, *45*, 76–85.

Veneziano, D., and C. Lepore (2012), The scaling of temporal rainfall, *Water Resour. Res.*, *48*, W08516, doi:10.1029/2012WR012105.

Venugopal, V., S. G. Roux, E. Foufoula-Georgiou, and A. Arneodo (2006), Revisiting multifractality of high-resolution temporal rainfall using a wavelet-based formalism, *Water Resour. Res.*, *42*, W06D14, doi:10.1029/2005WR004489.

Verrier, S., L. de Montera, L. Barthès, and C. Mallet (2010), Multifractal analysis of African monsoon rain fields, taking into account the zero rain-rate problem, *J. Hydrol.*, *389*(1-2), 111–120.

Verrier, S., L. Barthès, and C. Mallet (2013), Theoretical and empirical scale dependency of Z-R relationships: Evidence, impacts, and correction, *J. Geophys. Res.*, *118*, 7435–7449, doi:10.1002/jgrd.50557.